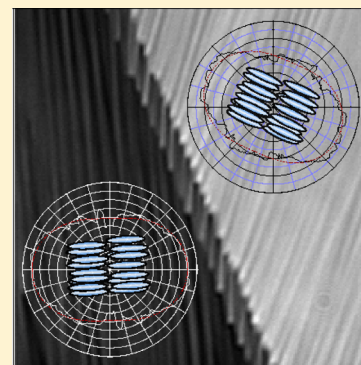


Slow Single-Molecule Diffusion in Liquid Crystals

Martin Pumpa and Frank Cichos*

Molecular Nanophotonics, Institute of Experimental Physics I, University of Leipzig, 04103 Leipzig, Germany

ABSTRACT: We report on measurements of single-molecule Brownian motion in liquid crystals, unravelling the anisotropic mobility of individual dye molecules. This anisotropic Brownian motion is directly correlated with the structural properties in a smectic A (8CB) and a nematic (5CB) liquid crystal sample cell on the micrometer scale using polarization contrast microscopy. A considerably slower mobility of dye molecules is found as compared to self-diffusion measurements by NMR, while anisotropy values compare well to recent literature data. This is suggested to be related to local distortions of the director structure around the dye molecules.



INTRODUCTION

Liquid crystals play an important role in many applications due to their optical properties. For most applications in switchable photonic devices,¹ the unique relation between optical, structural, and dynamical properties of these materials is of critical importance. Liquid crystals obey a distinct orientational order in an otherwise flowing spatial arrangement of molecules. The preferred spatial direction of alignment is called the director. Materials of this kind show a rotational symmetry around the director. The dynamical properties should therefore also reflect the same kind of symmetry. Accordingly, different values for the mobility along and perpendicular to the director have been found.^{2–6} NMR experiments on 8CB and 5CB, for example, have investigated the self-diffusion of the liquid crystal molecules,^{7–9} where the anisotropy of mobility was determined in a wide temperature range, reaching values up to 2.5 for 5CB and 2 for 8CB. Other experimental techniques applied to nematics include single-molecule fluorescence correlation measurements (FCS)¹⁰ and the fluorescence recovery after photobleaching (FRAP) on thin free-standing films of a liquid crystal.¹¹ Results on the time-dependent concentration spreading of dye-doped particles in 5CB¹² and on forced Rayleigh scattering (FRS)^{13–17} have been reported as well. Most of these methods, however, detect averaged properties of the liquid crystal from large prealigned sample regions, determined over long periods of time or at large particle ensembles. Self-diffusion measurements on single liquid-crystalline structures by a tracking technique have been carried out on macroscopic rod-like viruses, where the motion of single labeled components is monitored using fluorescence microscopy in the isotropic and nematic phases¹⁸ and the smectic phase as well.¹⁹ Recently, also single macroscopic particles have been used to determine the viscous properties in liquid crystal cells. For example, the drag force in liquid crystals has been studied for spherical colloidal particles, immersed in a nematic phase.^{20,21} In this suspension, the surface properties of the embedded particles can cause

reorientation of the liquid crystal director in close proximity to the colloid.^{22–24} Radial and tangential anchoring is reported, and different defect structures in the director field arise around the particles, depending on the strength of the interaction. In addition to a displacement of the original director lines, these strong director distortions close to the particle constantly change the local orientation of the liquid crystal molecules when the colloid diffuses. This causes an additional friction term to appear from the rotational viscosity as compared to a surrounding with constant uniform director orientation.^{24–27}

Here, we report on single-molecule tracking (SMT) measurements in a liquid crystal, where the probe molecules are of comparable size to their liquid-crystalline host. It is thus expected that the mobility of the fluorescent tracers reveals the same anisotropy as the host molecule diffusion and thus reflects the self-diffusion of the liquid crystal without any contribution by a distortion due to director reorientation to the viscosity. To determine the orientation of the director in our liquid crystal cell, we employ a method based on polarization microscopy, enabling us to carry out the experiments with single fluorescent molecules in sections where the alignment is known and without the use of external fields. A much slower but anisotropic diffusion of dye molecules is found and suggested to be related to local structural distortions in the liquid crystal.

EXPERIMENTAL TECHNIQUES

Setup and Sample Preparation. Single-molecule diffusion and liquid crystal structure have been studied in a home-built wide-field microscopy setup. The setup joins two detection modes, a fluorescence mode for single-molecule imaging and a polarization mode for orientational imaging. Both modes can be switched without the need to move the

Received: July 26, 2012

Revised: October 16, 2012

Published: October 19, 2012

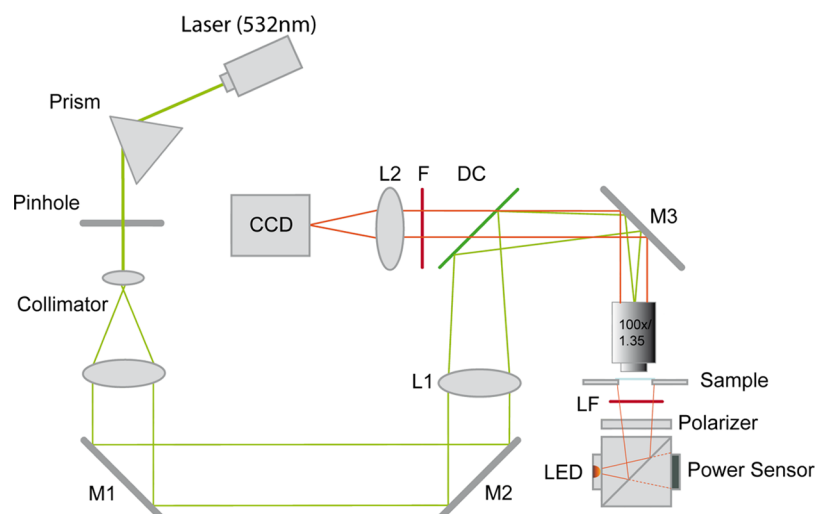


Figure 1. Single-molecule fluorescence microscope with a 532 nm excitation laser (Pusch Optics); M1–M3 are broad-band mirrors (Thorlabs), L1 and L2 are achromatic lenses (Thorlabs), and F denotes either a set of filters for fluorescence imaging or a polarization filter if the microscope is used in polarization contrast mode. DC stands for a dichroic mirror (XF21017, Omega Optical). In polarization contrast mode, the sample is illuminated by a red light LED. The light passes a beam splitter, a polarizer, and a laser-line filter (LF) at 632.8 nm. An optical power sensor behind the beam splitter monitors the intensity of the LED. Images are projected onto a frame transfer CCD camera (Roper Scientific S12F).

sample. The imaged area stays the same. This allows a direct correlation of liquid crystal structure and tracer dynamics.

Fluorescence Mode. The wide-field fluorescence mode employs a solid-state DPSS laser (Pusch Optics, 532 nm) to excite the fluorescence of the molecular tracers (see Figure 1). The excitation laser is coupled into the setup by a dichroic mirror and focused to the backfocal plane of the microscope objective (Olympus 100/1.3). Fluorescent light is collected by the same objective and imaged to a frame transfer CCD (Roper scientific S12F) by a 200 mm tube lens. Residual excitation light is removed from the emission by a set of interference filters (band-pass filter HQ545 LP, Edmund, and a long-pass filter 595AF60, Omega Optical). All single-molecule measurements have been carried out with an exposure time of 20 ms and a frame rate of 25 Hz. Each measurement consists of several videos (15–20) with 1000 frames each. A standard tracking algorithm developed in our lab is used to obtain trajectories of individual dye molecules. Single-molecule positions are found by fitting a two-dimensional Gaussian to each fluorescent spot in each frame. Single-molecule diffusion steps are connected by a nearest-neighbor detection between subsequent frames.

Polarization Mode. For recording polarization-resolved images, the microscope is equipped with a red light LED source below the sample, as shown in Figure 1. The LED light passes a polarization filter before the sample. The transmitted light is collected by the microscope objective and filtered by a laser-line filter ($\lambda = 632.8$ nm, Omega Optical) and a second polarizer (analyzer), which can be rotated with respect to the incident light polarization. To switch to fluorescence detection, the analyzer and band-pass filter are removed and replaced by the corresponding filters for fluorescence detection. The LED is turned off for single-molecule imaging.

Samples. Thin films of 8CB (4-*n*-octyl-4-cyanobiphenyl, Merck) and 5CB (4-*n*-pentyl-4-cyanobiphenyl, Merck) doped with PDI (Perylene Diimide, Sigma Aldrich) at nanomolar concentration were prepared between two glass coverslips (0.1 mm thickness). To ensure uniform, parallel alignment of the liquid crystal molecules, both slides have been coated with a

polyvinyl alcohol (PVA) film and rubbed with lens-cleaning tissue.^{28–30} The resulting liquid crystal film thickness can be calculated from the optical retardation β of the cell that will be introduced later. It is below 1 μm , so that no defocusing of the tracer molecules occurs during particle tracking. The 8CB liquid crystal sample is found to be in the smectic A phase and the 5CB sample in the nematic phase under the experimental conditions at $T = 297$ K.

Single-Molecule Data Analysis. The Brownian motion of single molecules in isotropic fluids leads to a Gaussian probability density distribution for finding a molecule at a position \mathbf{r} after a time lag τ . The corresponding probability density distribution is given by

$$p(\mathbf{r}, \tau) = \frac{1}{(4\pi D\tau)^{3/2}} \exp\left(-\frac{\mathbf{r}^2}{4D\tau}\right) \quad (1)$$

where D is the isotropic diffusion coefficient. In the case of an anisotropic Brownian motion, D becomes a 2nd rank tensor \mathbf{D} , and the resulting probability distribution is

$$p(\mathbf{r}, \tau) = \frac{1}{\sqrt{|\mathbf{D}|4\pi\tau}^3} \exp\left(-\frac{\mathbf{r}^T \mathbf{D}^{-1} \mathbf{r}}{4\tau}\right) \quad (2)$$

Thus, the spherically symmetric density distribution for the isotropic case will be distorted to an ellipsoidal probability distribution. If we assume two-dimensional anisotropic diffusion in a thin film, the tensor has only two independent principal components, which become accessible by analyzing the probability density distribution for the displacement in the two dimensions. If the distribution is analyzed in terms of projecting the displacement vector \mathbf{r} to a given direction characterized by the unit vector $\mathbf{e} = \{\cos(\phi), \sin(\phi)\}$, then the projected displacement distribution resembles a one-dimensional Brownian motion along the unit vector direction with an effective diffusion coefficient ($\mathbf{e}^T \mathbf{D} \mathbf{e}$). The density distribution of this projected Brownian motion is

$$p(\mathbf{r}, \mathbf{e}, \tau) = \frac{1}{\sqrt{4\pi\mathbf{e}^T\mathbf{D}\mathbf{e}\tau}} \exp\left(-\frac{(\mathbf{r}\cdot\mathbf{e})^2}{4\mathbf{e}^T\mathbf{D}\mathbf{e}\tau}\right) \quad (3)$$

which changes its width $\sigma(\tau)$ with the orientation of the vector \mathbf{e} according to

$$\sigma^2(\tau) = 2\tau\mathbf{e}^T\mathbf{D}\mathbf{e} \quad (4)$$

Equation 4 corresponds to the mean-square displacement along the unit vector direction \mathbf{e} for a certain time lag τ . If the principle components of the tensor \mathbf{D} are denoted by D_{\parallel} and D_{\perp} , eq 4 can be transformed into

$$\sigma^2(\tau, \phi) = 2\tau(D_{\parallel} \cos^2(\phi - \phi_0) + D_{\perp} \sin^2(\phi - \phi_0)) \quad (5)$$

inserting the unit vector $\mathbf{e} = \{\cos(\phi), \sin(\phi)\}$. The angle ϕ_0 is subtracted from the argument to allow for a possible rotation of the diffusion tensors principle components (i.e., the fast diffusion axis) in the observation plane relative to the laboratory reference frame. According to eq 3, we can analyze the anisotropic motion of single dye molecules embedded in a nematic or smectic liquid crystal by projecting their displacement vector $\Delta\mathbf{r} = \mathbf{r}(t) - \mathbf{r}(t - \tau)$ between two frames separated by a time τ on a direction given by the unit vector \mathbf{e} , resulting in

$$\Delta x(\tau) = [\mathbf{r}(t + \tau) - \mathbf{r}(t)] \cdot \mathbf{e} \quad (6)$$

The projected displacements Δx shall then obey a Gaussian probability density distribution, and its width σ_D reveals the projected diffusion coefficient along the direction \mathbf{e} . The width, however, only in the ideal case of infinitely short exposure times without any noise, does correspond to eq 5. In a real experiment, the finite exposure time Δt_{exp} as well as detection/shot noise lead to a finite localization accuracy. The finite exposure time Δt_{exp} leads to a single-molecule image that is a convolution of the point spread function of the imaging system and the trajectory of the Brownian motion during Δt_{exp} . The apparent particle position in each frame therefore depends on the exposure time. This inaccuracy has been considered by Montiel et al.³¹ Accordingly, the displacement distribution delivers

$$p_{\text{obs}}(\Delta x) = \frac{1}{2\pi\sigma_{\text{obs}}^2} \exp\left(-\frac{\Delta x^2}{2\sigma_{\text{obs}}^2}\right) \quad (7)$$

with $\sigma_{\text{obs}}^2 = 2D(1 - \Delta t_{\text{exp}}/3\Delta t_{\text{frame}})\Delta t_{\text{frame}}$, where Δt_{frame} is the inverse frame rate. In addition to Brownian motion during the exposure, adsorbed single molecules at the solid surface are captured in the videos. Thus, the actual distribution of projected displacements is the sum of two Gaussian distributions (as shown in Figure 2), one for the adhered and the other one for diffusing molecules. The width of the Gaussian distribution of the immobile molecules leads to the localization accuracy σ_{loc} , which is determined by the signal-to-noise ratio. In the present setup, the localization accuracy is found to be $\sigma_{\text{loc}} = 63$ nm, resulting in a lower bound for detectable mobilities of $D_{\text{min}} = 6 \times 10^{-14}$ m²/s at an inverse frame rate of $\Delta t_{\text{frame}} = 40$ ms with an exposure time of $\Delta t_{\text{exp}} = 20$ ms. The width of the Gaussian distribution of the mobile fraction of molecules then delivers the diffusion coefficient along the projection direction, as detailed above. Due to the finite localization accuracy, the error for all determined diffusion coefficients is at least $\Delta D_{\text{loc}} = (2\sigma_{\text{loc}})^2/2\Delta t_{\text{frame}} = 0.2 \times 10^{-12}$ m²/s.

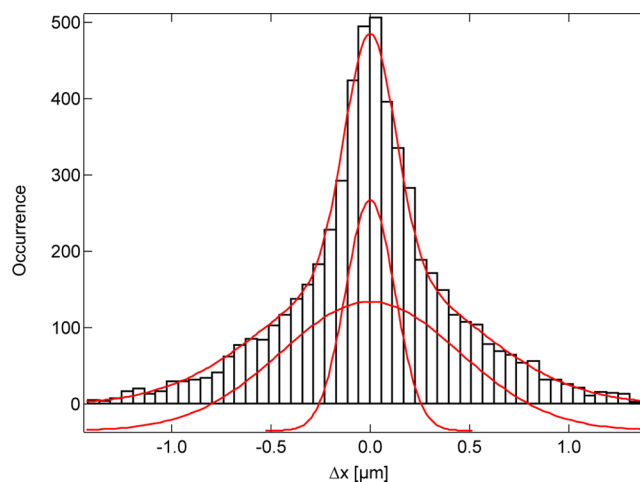


Figure 2. Step size distribution of 11000 steps of single molecules diffusing in 8CB. The steps have been projected along an arbitrary direction and fitted with the sum of two Gaussian distributions. The narrow central peak corresponds to the contribution of immobile dye molecules that are adhered to the polymer surface for a short time during the measurement.

Overall, the analysis of the displacement distribution for a set of different directions \mathbf{e} delivers the magnitude and orientation of the diffusion tensors principle axes D_{\parallel}, D_{\perp} . As described by Schob et al.,³² the advantage of the above-presented analysis is that it can be applied to any subensemble of molecules, for example, different spatial regions in a sample, as well as every direction \mathbf{e} and time interval Δt_{frame} . Here, we apply this technique to determine the anisotropic Brownian motion in different spatial areas of our liquid crystal samples.

Liquid Crystal Orientation Analysis. The orientation of the director \mathbf{S} in the mesophases of a uniaxial liquid crystal can be determined by polarization contrast microscopy. Due to the rubbing of the confining PVA surfaces of the liquid crystal cell, we assume the director to be oriented parallel to the glass slides. The homeotropic alignment of the dielectric building blocks results in birefringent optical properties of the liquid crystal cell. When placed between two polarizers, the intensity transmitted by the cell depends on the orientation α of the analyzer, the orientation δ of the polarizer, and the optical properties of the liquid crystal sample (see Figure 3 for a sketch).

Recording the intensity transmitted through the polarizers and liquid crystal cell at varying polarizer angles allows determination of the orientation of the director \mathbf{S} in the sample. Following refs 33 and 34 and assuming that there is no

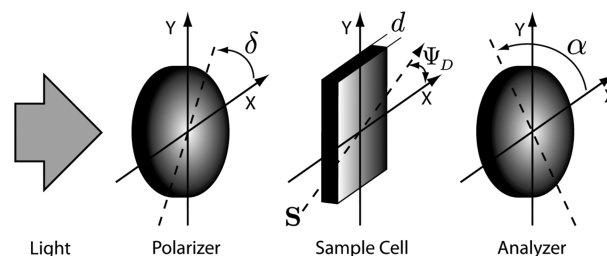


Figure 3. Sketch of a polarization contrast setup. Transmitted intensities depend on the cell thickness d , the director orientation angle Ψ_D , and the angular position δ and α of the polarizer and analyzer within the laboratory frame.

twist of the director in the sample cell, eq 8 is obtained for the transmission T of the sample

$$T(\alpha, \delta) = \cos^2(|\beta|) \cos^2(\delta - \alpha) + \sin^2(|\beta|) \cos^2(\delta + \alpha - 2\Psi_D) \quad (8)$$

Here, Ψ_D is the director orientation angle, and $\beta = \pi d \Delta n / \lambda$ is the phase retardation within a cell of thickness d . The birefringence of the liquid crystal is $\Delta n = n_e - n_o$, and λ denotes the wavelength of the incident light. Note that the transmission T is normalized and ranges between values of 0 and 1, indicating no or complete transmission. In the cases when the polarizer and analyzer are oriented either perpendicularly or parallel to each other, eq 8 simplifies to

$$T_c = T(\alpha = \delta + \pi/2) = \sin^2(|\beta|) \sin^2(2\delta - 2\Psi_D)$$

$$T_p = T(\alpha = \delta) = \cos^2(|\beta|) + \sin^2(|\beta|) \cos^2(2\delta - 2\Psi_D) \quad (9)$$

and can be easily applied to determine the liquid crystal director orientation. We recorded the transmitted intensities for polarizer orientations in an interval of $\delta \in [0, \pi)$ in steps of $\pi/18$ (corresponding to 10°) while staying in the crossed or parallel configuration, respectively. The data have been normalized to $T_c + T_p = 1$ and was then fitted with eq 9. The values of β and Ψ_D are extracted from those fits. Because the retardation β changes periodically with thickness d of the liquid crystal sample ($\beta(d) = \beta(d + \lambda)$), the fit has been restricted to a range of $\beta \in [0, \dots, \pi)$. Note that the result for Ψ_D is inherently invariant against rotation by $\pi/2$ (i.e., $T(\Psi_D + \pi/2) = T(\Psi_D)$). Intensity values are gathered for each pixel in the camera image, which allows calculation of the orientation of the liquid crystal director for all imaged positions in the sample. Furthermore, polarization imaging and single-molecule tracking are carried out in the same spatial area without any sample realignment. Thus, structural information obtained from the polarization images can be directly correlated to information on the anisotropic mobility of probe molecules in distinct areas of the liquid crystal matrix.

RESULTS AND DISCUSSION

A typical polarization image of an 8CB sample area at room temperature ($T = 297$ K) is shown in Figure 4. It is clearly visible that the intensity is not homogeneous throughout the image and divides this part of the sample in two well-distinguishable areas with different optical properties. The fine structure in the polarization contrast picture gives a first idea on the difference in structural alignment of the liquid crystal and is also typical for a smectic liquid crystal phase. The orientation in the two regions is stable upon temperature cycling to the isotropic phase and returning to the nematic phase. This suggests that the alignment of the liquid crystal is surface induced.

The analysis of the polarization contrast measurement has been done for every pixel of the image, resulting in a map of local structural properties. Each pixel averages the director orientation over a region of (144×144) nm². The results are displayed in Figure 5. Histograms of the calculated values of the director orientation, as shown in Figure 6, confirm the presence of two distinct sample areas with different mean director orientations, which will be denoted as area A_1 and A_2 in the following (see Figure 4).

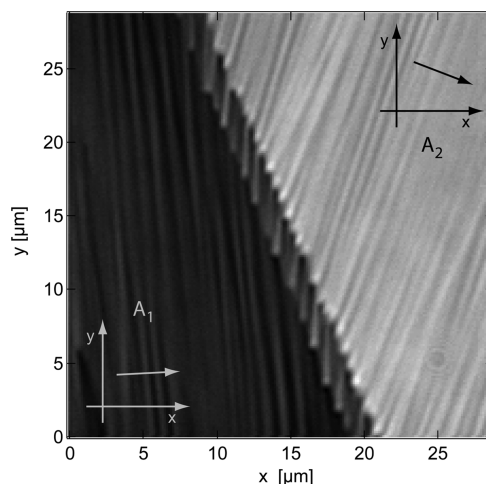


Figure 4. Polarization contrast picture of an 8CB sample. The image has been recorded at room temperature $T = 297$ K with crossed polarizers ($\alpha = \delta + \pi/2$). Different intensities and the striped structure indicate different orientations of the liquid crystal director Ψ_D . The two arrows indicate the director orientations in the corresponding regions A_1 and A_2 .

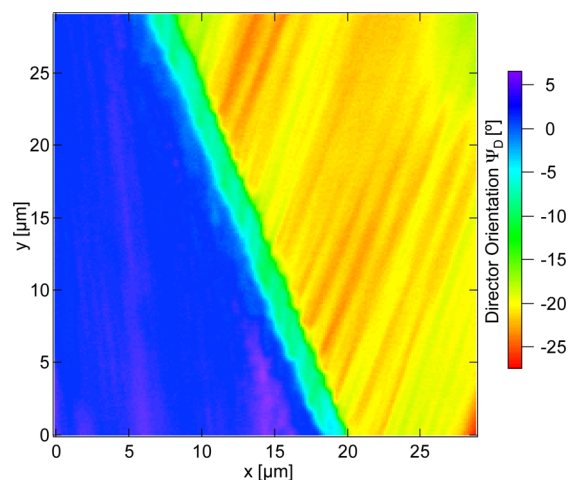


Figure 5. Calculated angles for the orientation of the director Ψ_D in the region depicted in Figure 4. The director orientation is perpendicular to the striped texture in the images. Two well-separated areas with different director orientations are found.

Two major director angles are observed, which are given by $\Psi_D^{A_1} = (3 \pm 1)^\circ$ in area A_1 and $\Psi_D^{A_2} = (-21 \pm 1.5)^\circ$ in area A_2 . Furthermore, a minor peak at about $\Psi_D = -8^\circ$ is found, which corresponds to the region between area A_1 and A_2 , as visible in Figure 6. Because only a very small portion of the sample contains this director orientation, we refrain from a detailed discussion of single-molecule diffusion in this area.

The retardations found in the two sample areas are about $\beta^{A_1} = 0.380 \pm 0.016$ and $\beta^{A_2} = 0.45 \pm 0.04$. Given an optical anisotropy of 8CB at room temperature ($T = 297$ K) of $\Delta n = 0.17$,³⁵ we calculate the cell thicknesses to be $d_{A_1} = (448 \pm 19)$ nm and $d_{A_2} = (532 \pm 48)$ nm. If we assume equal mean order parameters in all pictured regions, this thickness difference may have been caused by the mechanical treatment of the PVA surfaces.

While the director angle histograms discriminate between sample areas of different structural properties, even within each

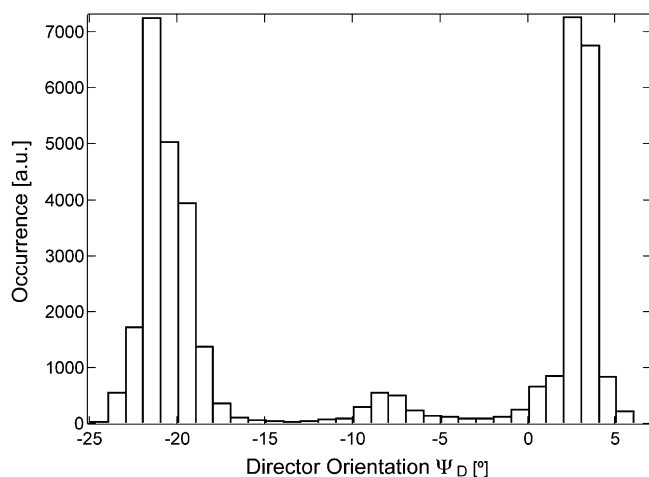


Figure 6. Histogram over all values of Ψ_D in Figure 5. The two main peaks are assigned to the two distinct spatial regions visible in Figures 4 and 5. The mean values of calculated director orientation are $\Psi_D^{A_1} = (3 \pm 1)^\circ$ in area A_1 and $\Psi_D^{A_2} = (-21 \pm 1.5)^\circ$ in area A_2 . The minor peak at around $\Psi_D = -8^\circ$ corresponds to the region between area A_1 and A_2 and is omitted in the discussion.

area, distributions of director orientations are revealed that do not result only from the fitting errors. They are characteristic for the smectic phase and possibly related to the surface roughness of the rubbed PVA film. Similar measurements have been carried out on 5CB samples (data not shown). The considered sample area contains a single well-oriented liquid-crystalline domain. The analysis of the polarization images revealed values of $\beta^{5CB} = 0.89 \pm 0.15$ with a director orientation angle of $\Psi_D^{5CB} = (89 \pm 5)^\circ$ and a liquid crystal cell thickness of $d_{5CB} = (994 \pm 178)$ nm.

When switched to fluorescence mode, the Brownian motion of single PDI molecules in the sample area can be observed. The projected step size distributions of the detected single molecules have been analyzed as described above separately for each of the two areas A_1 and A_2 of the 8CB sample. In area A_1 , 6508 individual steps of single molecules were recorded. In area A_2 , 3470 single-molecule steps were used for the step size analysis. The calculated angular dependence of the diffusion coefficients is shown in Figure 7. The graphs display a clear anisotropic mobility. The fast and slow diffusion tensor axes at

orientations ϕ_0 and $\phi_0 + 90^\circ$ are determined by fitting the angle-dependent mobility curves with

$$D(\phi) = D_{\parallel} \cos^2(\phi - \phi_0) - D_{\perp} \sin^2(\phi - \phi_0) \quad (10)$$

In area A_1 , the fast axis is found at an angle of $\phi_0^{A_1} = (1.5 \pm 0.5)^\circ$ with a diffusion coefficient $D_{\parallel}^{A_1} = 4.5 \times 10^{-12} \text{ m}^2/\text{s}$, while $D_{\perp}^{A_1} = 2.9 \times 10^{-12} \text{ m}^2/\text{s}$.

In area A_2 , the fast axis is at $\phi_0^{A_2} = (-23.7 \pm 0.8)^\circ$ with $D_{\parallel}^{A_2} = 4.3 \times 10^{-12} \text{ m}^2/\text{s}$ and $D_{\perp}^{A_2} = 2.8 \times 10^{-12} \text{ m}^2/\text{s}$ along the slow axis. For both areas, the standard deviation of the experimental data with respect to the fitted curve is $\Delta D_{\text{fit}} = 0.2 \times 10^{-12} \text{ m}^2/\text{s}$. The values of the diffusion tensors principle axes reveal a diffusion anisotropy of $D_{\parallel}/D_{\perp} = 1.5 \pm 0.2$ for both areas. Note that this value follows from a microscopic observation on individual liquid crystal domains, which obey a surface-induced order. It compares well to recent NMR data,⁹ where the liquid crystal has been aligned by external fields.

The analysis of the step size distributions of 11258 single steps in the 5CB liquid crystal sample delivers diffusion coefficients of $D_{\parallel}^{5CB} = 5.75 \times 10^{-12} \text{ m}^2/\text{s}$ and $D_{\perp}^{5CB} = 8.47 \times 10^{-12} \text{ m}^2/\text{s}$ with a fitting error of $\Delta D_{\text{fit}} = 0.01 \times 10^{-12} \text{ m}^2/\text{s}$ (see Figure 8). These values correlate well with the results of FRAP experiments in 5CB in the literature.¹¹ The anisotropy of mobility is determined to be $D_{\parallel}/D_{\perp} = 1.5 \pm 0.2$ with the fast axis oriented at an angle of $\phi_0^{5CB} = (91.5 \pm 0.1)^\circ$. Polarization measurements reveal a director orientation of $\Psi_D = (89 \pm 5)^\circ$, which is in good agreement with the orientation of the fast axis for recent NMR studies of 5CB.⁹ A summary of all measured orientation and diffusion properties is listed in Table 1.

Despite the good agreement of the anisotropy values, the absolute values of the diffusion tensors' principle components deviate strongly from NMR^{8,36,37} and FRS data.^{16,38} Our experimental single-molecule diffusion data are about a factor of 5 times smaller than the literature results. NMR experiments carried out on bulk samples of our liquid crystal systems in the isotropic phase further confirm the literature NMR diffusion coefficients ($D(5CB, T = 311.0 \text{ K}) = 6.8 \times 10^{-11} \text{ m}^2/\text{s}$ and $D(8CB, T = 320.4 \text{ K}) = 6.5 \times 10^{-11} \text{ m}^2/\text{s}$). Therefore, we expect the single-molecule tracer to play an important role in the observation of the slow diffusion.

A deviation from bulk diffusion coefficients may be caused by the fact that our experiments are carried out in thin films of liquid crystals with film thickness values below $1 \mu\text{m}$, while all

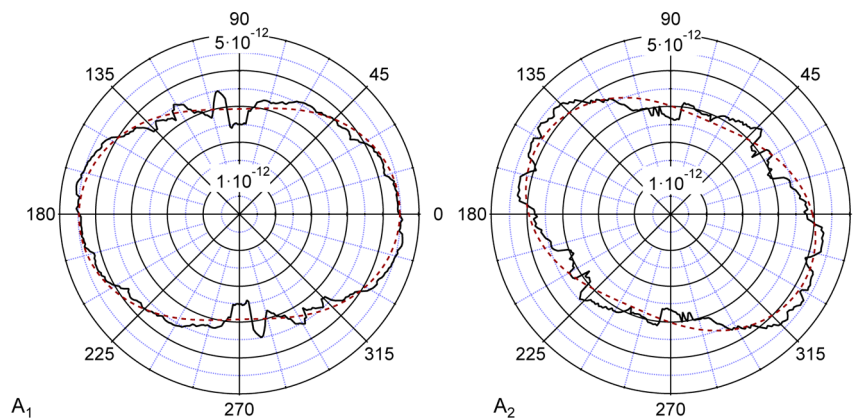


Figure 7. Angle-dependent diffusion coefficient calculated from single-molecule step size distributions in the areas A_1 (left) and A_2 (right) in Figure 4. The dashed line is a fit using eq 10. The angle of fastest mobility ϕ_0 correlates well with the mean director orientation calculated in each region ($\phi_0^{A_1} = (1.5 \pm 0.5)^\circ$ with $\Psi_D^{A_1} = (3 \pm 1)^\circ$ and $\phi_0^{A_2} = (-23.7 \pm 0.8)^\circ$ with $\Psi_D^{A_2} = (-21 \pm 1.5)^\circ$ in area A_2).

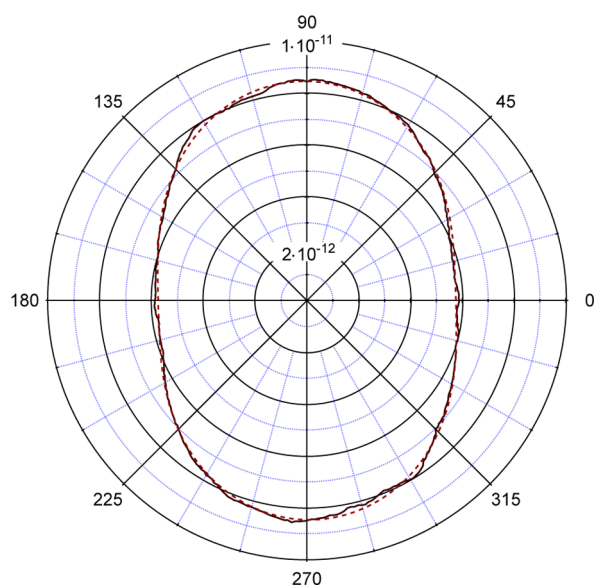


Figure 8. Angle-dependent diffusion coefficient calculated from the determined single-molecule step size distributions measured on a 5CB sample at $T = 297$ K. The dashed line is a fit using eq 10. The direction of the fast mobility axis is $\phi_0^{\text{5CB}} = (91.5 \pm 0.1)^\circ$. This value correlates well with the mean director orientation determined from polarization measurements of $\Psi_D = (89 \pm 5)^\circ$.

Table 1. Summarized Results of Single-Molecule Diffusion Measurements in Comparison with the Director Orientation Ψ_D Determined from Polarization Contrast Measurements^a

	Ψ_D in $^\circ$	ϕ_0 in $^\circ$	D_{\parallel} in 10^{-12} m ² /s	D_{\perp} in 10^{-12} m ² /s
area 1	3 ± 1	1.5 ± 0.5	4.5 ± 0.4	2.9 ± 0.4
area 2	-21 ± 1.5	-23.7 ± 0.8	4.3 ± 0.4	2.8 ± 0.4
5CB	89 ± 5	91.5 ± 0.1	8.5 ± 0.2	5.8 ± 0.2

^aThe angle ϕ_0 depicts the orientation of the measured diffusion tensor with its principal components D_{\parallel} and D_{\perp} .

NMR and FRS experiments are using bulk material. The motion of suspended particles or molecules can be highly influenced by the hydrodynamic no-slip boundary conditions in the vicinity of confining walls.^{32,39–43} Because we are observing only two-dimensional trajectories and therefore average over all possible positions perpendicular to the surfaces, this would lead to a slower apparent mobility, as indeed observed. However, according to the literature on LC,^{11,44–46} confinement effects on the mobility can be neglected in sample cells that are much thicker than the molecular radius of a single LC molecule. Thus, for a LC film thickness of several hundred nanometers, we expect only minor influence of the interfaces on the mean diffusion coefficient in the film.

At second glance, single-molecule tracking is only suitable if the diffusion coefficients to be observed are within a certain range, which is determined by the camera speed and the number of emitted photons. Fast single-molecule diffusion as compared to the frame rate spreads the emitted number of photons over larger regions of the CCD, thus decreasing the peak number of photons. This decreases the signal-to-noise ratio, and the molecule may not be reliably identified in front of the background noise. To exclude the existence of such an unidentified fast single-molecule dynamics of PDI in 5CB and 8CB, we performed fluorescence recovery after photobleaching (FRAP) measurements in a different setup. As compared to the

single-molecule samples, we have used a higher content of dye molecules in the liquid crystal, such that a homogeneous emission is observed. The details of the setup and data analysis are described in ref 11. The FRAP setup has been tested by examining the diffusion of R6G in glycerine and glycerine/water mixtures. Pure glycerine has a viscosity of 987 mPa·s at room temperature $T = 297$ K, and assuming a hydrodynamical radius for R6G of 5.89 Å (as measured in ref 47), the Stokes–Einstein relation gives a theoretical diffusion coefficient of 0.374×10^{-12} m²/s. This value compares well to the one obtained from our test FRAP measurement (see Table 2). To mimic the

Table 2. Measured Mean Diffusion Coefficients with Experimental Uncertainty ΔD (in units of 10^{-12} m²/s) from FRAP experiments at $T = 297$ K

	D_{FRAP}	D_{theo}	ΔD
R6G in glycerine	0.38	0.37	0.01
R6G in glycerine/water	9.5	10.0	0.1
PDI in 5CB	2.6		0.8
PDI in 8CB	3.2		0.6

mean viscosity of 5CB, we have further prepared a glycerine/water mixture to yield a diffusion coefficient of $D = 1 \times 10^{-11}$ m²/s (94 wt % glycerine in water; viscosity: 36.4 mPa·s⁴⁸). FRAP experiments on this mixture also deliver results that are in good agreement with the Stokes–Einstein predictions, as displayed in Table 2. Together with the results of SMT experiments, this confirms the capability of both methods and our experimental setups to detect mobilities as they are predicted by NMR and FRS measurements. This suggests that the observed slow molecular diffusion of PDI in 5CB and 8CB must be related to the interaction of the dye molecule with the liquid crystal.

The dye molecules actually represent a defect in the liquid crystal due to the altered intermolecular interactions. The director structure around the dye molecule is deformed by the presence of such a defect. Molecular motion requires a reorientation of the director structure, leading to a larger effective viscosity around the dye molecule. Such effects have been recently discussed for the motion of spherical particles through the nematic phase of a liquid crystal.^{22,25,26} Depending on the strength of anchoring of the LC molecules at the particle surface, the particles distort the local director orientation. The reorientation of the LC molecules results in a change of effective viscosity that alters the diffusion coefficient of the probe colloid. Despite this change in the local viscosity, the values for the anisotropy of diffusion and viscosity are almost unchanged as compared to the undisturbed liquid crystal structure. Such distortions would thus only be visible in measurements of the absolute mobility of probes and not when determining the anisotropy of diffusion. As we have excluded other experimental issues, we suggest that the slow diffusion observed for the dynamics of single PDI molecules in 5CB and 8CB in conjunction with a reasonable anisotropy is related to a deformation of the local director structure around the dye molecules.

CONCLUSION

Our studies focused on the spatially resolved mobility of single PDI molecules in a smectic A phase of the liquid crystal 8CB as well as the nematic phase of 5CB at room temperature. We analyzed the mobility of individual dye molecules by single-

molecule tracking experiments. The optical parameters of our liquid crystal film have been determined by means of polarization contrast microscopy. This allows a direct comparison of the dynamical properties reported by the dye molecules to the structural properties of the liquid crystal. The single-molecule tracking results reveal an anisotropic mobility that correlates well with the director orientation in the sample. The determined values of the principle axes of the diffusion tensors D_{\perp} and D_{\parallel} are 5 times smaller than the values found in recent self-diffusion by NMR experiments,^{8,37} while the diffusion anisotropy is in agreement with literature data. The rather strong deviation is attributed to local distortions of the liquid crystal director structure due to the presence of the dye molecule. Careful temperature-dependent measurements in the liquid-crystalline and isotropic phases shall give a more detailed insight into these structural distortions around the dye molecule.

AUTHOR INFORMATION

Corresponding Author

*E-mail: cichos@rz.uni-leipzig.de.

Notes

The authors declare no competing financial interest.

ACKNOWLEDGMENTS

We thank Dr. Valiulin for the NMR measurements. Financial support by the DFG Project CI-33/6-1 is acknowledged.

REFERENCES

- (1) Beeckman, J.; Neyts, K.; Vanbrabant, P. J. M. *Opt. Eng.* **2011**, *50*, 081202.
- (2) Chu, K.-S.; Moroi, D. S. *J. Phys. (Paris)* **1975**, *3*, 99.
- (3) Hess, S.; Frenkel, D. *Mol. Phys.* **1991**, *74*, 765–774.
- (4) Sollich, H.; Baalss, D.; Hess, S. *Mol. Cryst. Liq. Cryst.* **1989**, *168*, 189–195.
- (5) Hess, S.; Schwarzl, J. F.; Baalss, D. *J. Phys.: Condens. Matter* **1990**, *2*, SA279–SA284.
- (6) Franklin, W. *Phys. Lett. A* **1974**, *48*, 247–248.
- (7) Romanova, E. E.; Grinberg, F.; Pampel, A.; Kärger, J.; Freude, D. *J. Magn. Reson.* **2009**, *196*, 110–114.
- (8) Furó, I.; Dvinskikh, S. V. *Magn. Reson. Chem.* **2002**, *40*, 3–14.
- (9) Dvinskikh, S. V.; Furó, I.; Zimmermann, H.; Maliniak, A. *Phys. Rev. E* **2002**, *65*, 061701.
- (10) Kawai, T.; Kubota, A.; Kawamura, K.; Tsumatori, H.; Nakashima, T. *Thin Solid Films* **2008**, *516*, 2666–2669.
- (11) Bechhoefer, J.; Géminard, J.-C.; Bocquet, L.; Oswald, P. *Phys. Rev. Lett.* **1997**, *79*, 4922.
- (12) Hakemi, H. *Phys. Lett. A* **1983**, *95*, 35–37.
- (13) Hara, M.; Ichikawa, S.; Takezoe, H.; Fukuda, A. *Jpn. J. Appl. Phys.* **1984**, *23*, 1420–1425.
- (14) Urbach, W.; Hervet, H.; Rondelez, F. *J. Chem. Phys.* **1985**, *83*, 1877–1887.
- (15) Spiegel, D. R.; Thompson, A. L.; Campbell, W. C. *J. Chem. Phys.* **2001**, *114*, 3842–3847.
- (16) Nishikawa, T.; Minabe, J.; Takezoe, H.; Fukuda, A. *Mol. Cryst. Liq. Cryst.* **1993**, *231*, 153–161.
- (17) Hara, M.; Tenmei, H.; Ichikawa, S.; Takezoe, H.; Fukuda, A. *Jpn. J. Appl. Phys.* **1985**, *24*, L777–L780.
- (18) Lettinga, M. P.; Barry, E.; Dogic, Z. *Europhys. Lett.* **2005**, *71*, 692–698.
- (19) Grelet, E.; Lettinga, M.; Bier, M.; van Roij, R.; van der Schoot, P. *J. Phys.: Condens. Matter* **2008**, *20*, 494213.
- (20) Verhoeff, A. A.; van Rijssel, J.; de Villeneuve, V. W. A.; Lekkerkerker, H. N. W. *Soft Matter* **2008**, *4*, 1602–1604.
- (21) Loudet, J.; Hanuss, P.; Poulin, P. *Science* **2004**, *306*, 1525.
- (22) Terentjev, E. M.; Shiyankovskii, S. V.; Ruhwandl, R. W.; Kuksenok, O. V. *Phys. Rev. E* **1996**, *54*, 5198–5203.
- (23) Ruhwandl, R. W.; Terentjev, E. M. *Phys. Rev. E* **1996**, *54*, 5204–5210.
- (24) Stark, H.; Ventzki, D. *Phys. Rev. E* **2001**, *64*, 031711.
- (25) Stark, H. *Phys. Rep.* **2001**, *351*, 387–474.
- (26) Stark, H.; Ventzki, D. *Europhys. Lett.* **2002**, *57*, 60–66.
- (27) Stark, H.; Ventzki, D.; Reichert, M. *J. Phys.: Condens. Matter* **2003**, *15*, S191–S196.
- (28) Berreman, D. W. *Phys. Rev. Lett.* **1972**, *28*, 1683–1686.
- (29) Geary, J. M.; Goodby, J. W.; Kmetz, A. R.; Patel, J. S. *J. Appl. Phys.* **1987**, *62*, 4100–4108.
- (30) Kumar, S.; Kim, J.-H.; Shi, Y. *Phys. Rev. Lett.* **2005**, *94*, 077803.
- (31) Montiel, D.; Cang, H.; Yang, H. *J. Phys. Chem.* **2006**, *110*, 19763–19770.
- (32) Schob, A.; Pampa, M.; Selmeke, M.; Cichos, F. *J. Phys. Chem. C* **2010**, *114*, 4479–4485.
- (33) Soutar, C.; Lu, K. *Opt. Eng.* **1994**, *33*, 2704–2712.
- (34) Durán, V.; Lancis, J.; Tajahuerce, E.; Jaroszewicz, Z. *J. Appl. Phys.* **2005**, *97*, 043101.
- (35) Horn, R. G. *J. Phys.* **1978**, *39*, 105–109.
- (36) Kim, M. J.; Cardwell, K.; Khitrin, A. K. *J. Chem. Phys.* **2004**, *120*, 11327–11329.
- (37) Dvinskikh, S.; Furo, I. *Russ. Chem. Rev.* **2006**, *75*, 497–506.
- (38) Hara, M.; Takezoe, H.; Fukuda, A. *Jpn. J. Appl. Phys.* **1986**, *25*, 1756–1761.
- (39) Schob, A.; Cichos, F. *Chem. Phys. Lett.* **2010**, *484*, 192–196.
- (40) Faucheux, L.; Libchaber, A. *Phys. Rev. E* **1994**, *49*, 5158.
- (41) Lobry, L.; Ostrowsky, N. *Phys. Rev. B* **1996**, *53*, 12050.
- (42) Saugey, A.; Joly, L.; Barrat, J. L.; Bocquet, L. *J. Phys.: Condens. Matter* **2005**, *17*, S4075.
- (43) Benesch, T.; Yiaccoumi, S.; Tsouris, C. *Phys. Rev. E* **2003**, *68*, 021401.
- (44) Ji, Q.; Lefort, R.; Ghoufi, A.; Morineau, D. *Chem. Phys. Lett.* **2009**, *482*, 234–238.
- (45) Cramer, C.; Cramer, T.; Kremer, F.; Stannarius, R. *J. Chem. Phys.* **1997**, *106*, 3730–3742.
- (46) Schulz, B.; Tauber, D.; Friedriszik, F.; Graaf, H.; Schuster, J.; von Borczyskowski, C. *Phys. Chem. Chem. Phys.* **2010**, *12*, 11555–11564.
- (47) Müller, C. B.; Loman, A.; Pacheco, V.; Koberling, F.; Willbold, D.; Richtering, W.; Enderlein, J. *Europhys. Lett.* **2008**, *83*, 46001.
- (48) Cheng, N.-S. *Ind. Eng. Chem. Res.* **2008**, *47*, 3285–3288.